AIAA JOURNAL
Vol. 46, No. 1, January 2008

Technical Notes

TECHNICAL NOTES are short manuscripts describing new developments or important results of a preliminary nature. These Notes should not exceed 2500 words (where a figure or table counts as 200 words). Following informal review by the Editors, they may be published within a few months of the date of receipt. Style requirements are the same as for regular contributions (see inside back cover).

Comb Wings for Flapping Flight at Extremely Low Reynolds Numbers

D. Weihs* and E. Barta†
Technion—Israel Institute of Technology, 32000 Haifa, Israel

DOI: 10.2514/1.32500

Nomenclature

d	=	distance between two adjacent bodies within the row
e	=	ellipsoid eccentricity
l	=	rod half-length
m	=	number of rods within a row
p	=	pressure
s	=	a point along the rods axis
$\boldsymbol{u}$	=	velocity vector
u, v, w	=	components of velocity in the normal, n, tangential, s, and binormal, b, directions respectively
$\alpha_i^j(s), \beta_i^j(s)$	=	intensities of Stokeslets and doublets at point s
ε	=	slenderness ratio of an individual rod
μ	=	dynamical viscosity
ρ	=	density

I. Introduction

RECENT advances in microelectronics and communications technology have made millimeter-sized unmanned aerial vehicles (UAVs) feasible. Such vehicles are similar in size to insects, and therefore it is of interest to study the solutions that small insects have found for flying. The thrips family of insects has wingspans of order 1 mm (see Fig. 1) and exhibits unusual wings of comblike planform, with solidity ratios of 0.2 and less. We recently used this principle [1] to produce micro-aerodynamic decelerators with discontinuous surfaces.

An experimental study [2] of enlarged models of thrips wings has shown that the forces produced can be similar to those of solid wings, for $Re = \mathrm{o}(10)$. Recently, the authors have performed an analysis [3] calculating the flow around a row of slender ellipsoidal bodies moving with uniform and constant speed in creeping ($Re \ll 1$) flow. For spacing ratios (ratio of distance between neighboring rod axes to rod diameter) of up to 10, comb wings produce over 90% of the forces obtained on a continuous wing in gliding flight. This means that miniature aerodynamic decelerators can save up to 90% in weight while sacrificing only less than 10% in performance. This prediction strengthens our previous results [1] for bodies with surfaces consisting of two-dimensional netting with various solidity ratios, which sank at comparable speeds to continuous surfaces weighing over three times the net weights.

Here, flapping motions of comb wings, modeled by a finite row of slender bodies with different speeds depending on position in the row (see Fig. 2) are calculated based on the method presented in the next section. This provides a mathematical tool for the future design of small flapping wing UAVs based on thrips wings.

In this paper we calculate the flowfield around a finite row of slender bodies, in which the velocity of each rod is linearly proportional to the distance of the rod's center of mass from an arbitrary point along the line connecting these centers (Fig. 2), representing the "shoulder". This models a rigid comb wing consisting of rods perpendicular to the wing axis, flapping around a shoulder joint, that is, the wing root.

Motion in the three principal directions is calculated, describing a power stroke (normal flow), a feathered recovery stroke (tangential), and a possible retracting motion (binormal). Any combination of these can then be obtained by superposition.

II. Analysis

All existing solutions for multiple slender bodies in creeping flow [3–6] assume that the bodies all move with equal speed. However, flapping flight is characterized by a linear increase of the flapping velocities from the root of the wing (attached to the shoulder) to the wing tip. We calculate the forces on the rods constituting the wing and the velocities induced by them by distributing singularities (Stokeslets and doublets) along the rods' longitudinal axes. This results in a system of integral equations for the forces. This is a generalization of our previous work [3] on uniform speeds on the comb.

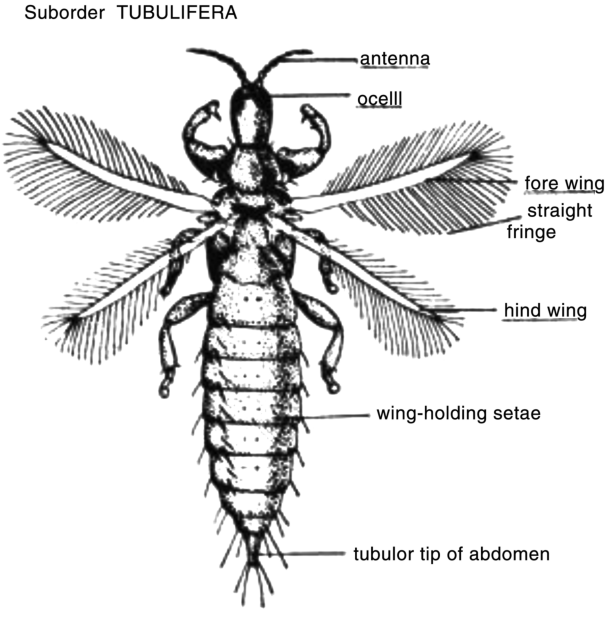

Fig. 1 Picture of a typical thrips [7].

Received 31 May 2007; revision received 30 August 2007; accepted for publication 12 September 2007.

*Distinguished Professor, Faculty of Aerospace Engineering.
†Senior Researcher, Faculty of Aerospace Engineering.

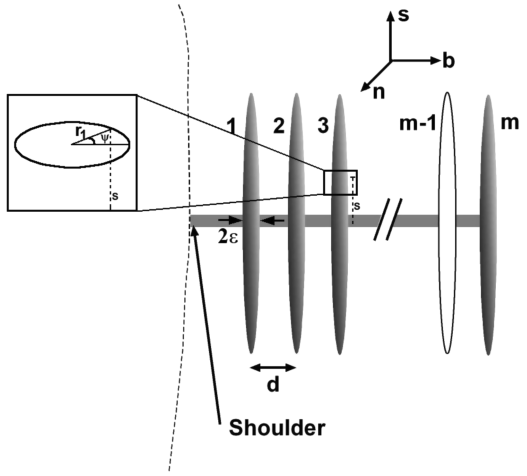

Fig. 2 Schematic description of the comb wing.

The calculation provides the forces on each rod, which essentially define the "leakiness" of the array (comb) as the forces are proportional to the local relative air speed. Thus, a rod with zero force means that it produces the same flow as a continuous wing, and a value of 0.04 means that there is a 4% loss of force relative to a section of continuous wing. Components of the forces are calculated in the three coordinates, as shown in Fig. 2:

n, normal: the direction normal to the comb plane;

s, tangential: the direction of the rods' longitudinal axes in the comb plane;

b, binormal: the direction of the wing span in the comb plane.

The normal component is obtained during the power stroke, that is, the wing is moved downwards while rotating around the shoulder. The tangential component appears where the wing is moved in the chordwise direction, that is, the wing is pulled back during the recovery stroke with the leading edge forward. The binormal component appears where the wing is pulled in the spanwise direction. Insects use combinations of these, with much more complex wing motions [7], both to gain unsteady effects not discussed in this paper and to minimize the loses due to the recovery stroke. The Stokes equations and the boundary conditions are linear, so that such complex motions can be described by combinations of the components calculated here. As already mentioned, the full mathematical model appears in [3], whereas here we present the relevant highlights and main points.

To obtain an analytical solution, we approximate the rods by extremely slender ellipsoids (see Fig. 2), thus enabling the use of singularities to describe the flowfield induced by a finite row of parallel rods immersed in an unbounded incompressible fluid moving at $Re \ll 1$ (Stokes flow). The motion can be in any direction relative to the ellipsoids. Motion of the row induces flow around and between the ellipsoids. This induced flow ranges far from the bodies due to the dominant viscous effects at the low Reynolds numbers considered. Normalizing all geometric measurements with respect to half body length, we define the slenderness ratio ε as the maximal radius of the ellipsoid and d as the distance between the centers of two adjacent bodies. We study cases where $1 \gg d \gg \varepsilon$. The number of rods m can be any integer from two upwards. We compute this flowfield to determine the range of parameters (ε, d, and m values) for which the ellipsoids will "drag" the fluid between them, and the flow over the whole row of slender bodies will approach that of a continuous surface.

The Stokes flow equations [8]

$$\nabla p = \mu \nabla^2 \bar{u} \tag{1}$$

$$\nabla \cdot \bar{u} = 0 \tag{2}$$

are solved for the velocity $\boldsymbol{u}$ and pressure p in a fluid with viscosity μ with given velocities. The equations are linear and so it is sufficient to solve for motions along the three orthogonal principal directions. Translation in any other direction is a linear combination of those three.

We use a coordinate system [8] that is tangential, normal, and binormal to the bodies' major axes $\mathbf{e}_s$, $\mathbf{e}_n$, and $\mathbf{e}_b$ (see Fig. 2). Each individual body is represented by a distribution of Stokeslets and doublets along its axis between its foci [3]. The intensities of these singularities are now found by imposing the no-slip condition at the rod surfaces, recalling that rod i is moving at velocities $v_i(s, r_1, \psi)$, $u_i(s, r_1, \psi)$, $w_i(s, r_1, \psi)$ along the $\mathbf{e}_s$, $\mathbf{e}_n$, and $\mathbf{e}_b$ directions at any arbitrary point (s, r_1, ψ) on the surface of each ellipsoid.

Denoting the intensities of the Stokeslets and doublets that are situated at point s on the axis of the ith ellipsoid ($i = 1, \ldots, m$) and act along the jth direction ($j = s$, n, or b) by $\alpha_i^j(s)$ and $\beta_i^j(s)$, respectively, and defining

$$e^2 = 1 - \varepsilon^2 \tag{3}$$

the relation between the Stokeslet and doublets strengths for each ellipsoid is given by [9]

$$\beta_i^j(s) = \frac{\varepsilon^2}{2} \alpha_i^j(s)(e^2 - s^2) \tag{4}$$

The velocities at point (s, r_1, ψ), that is, at the cross-sectional plane situated at height s that has the polar coordinates (r_1, ψ), are

$$\begin{aligned} u_i(s, r_1, \psi) \cong{}& (2L+1)\alpha_i^n(s) - \int_{-e}^{e} \frac{\alpha_i^n(s) - \alpha_i^n(s')}{|s - s'|}\, \mathrm{d}s' \\ &+ \sum_{\substack{j=1 \\ j \neq i}}^{m} \int_{-e}^{e} \frac{\alpha_j^n(s')}{\sqrt{(s-s')^2 + d_{ij}^2}}\, \mathrm{d}s' \\ &+ \frac{\varepsilon^2}{2} \sum_{\substack{j=1 \\ j \neq i}}^{m} \int_{-e}^{e} \frac{(e^2 - s'^2)\alpha_j^n(s')}{\sqrt{(s-s')^2 + d_{ij}^2}^3}\, \mathrm{d}s' \qquad i = 1, \ldots, m \end{aligned} \tag{5}$$

$$\begin{aligned} v_i(s, r_1, \psi) \cong{}& 2(2L-1)\alpha_i^s(s) - 2\int_{-e}^{e} \frac{\alpha_i^s(s) - \alpha_i^s(s')}{|s - s'|}\, \mathrm{d}s' \\ &+ \sum_{\substack{j=1 \\ j \neq i}}^{m} \int_{-e}^{e} \left\{ \frac{\alpha_j^b(s') d_{ij}(s - s')}{\sqrt{(s-s')^2 + d_{ij}^2}^3} \times \left(1 - \frac{3\varepsilon^2(e^2 - s'^2)}{2\{(s-s')^2 + d_{ij}^2\}}\right) \right. \\ &+ \left(1 + \frac{(s-s')^2}{\{(s-s')^2 + d_{ij}^2\}} \left[1 - \frac{3\varepsilon^2(e^2 - s'^2)}{2\{(s-s')^2 + d_{ij}^2\}}\right]\right) \\ &\left. \times \frac{\alpha_j^s(s')}{\sqrt{(s-s')^2 + d_{ij}^2}} \right\} \mathrm{d}s' \\ &+ \frac{\varepsilon^2}{2} \sum_{\substack{j=1 \\ j \neq i}}^{m} \int_{-e}^{e} \frac{(e^2 - s'^2)\alpha_j^s(s')}{\sqrt{(s-s')^2 + d_{ij}^2}^3}\, \mathrm{d}s' \qquad i = 1, \ldots, m \end{aligned} \tag{6}$$

$$\begin{aligned} w_i(s, r_1, \psi) \cong{}& (2L+1)\alpha_i^b(s) - \int_{-e}^{e} \frac{\alpha_i^b(s) - \alpha_i^b(s')}{|s - s'|}\, \mathrm{d}s' \\ &+ \sum_{\substack{j=1 \\ j \neq i}}^{m} \int_{-e}^{e} \left\{ \frac{\alpha_j^s(s') d_{ij}(s - s')}{\sqrt{(s-s')^2 + d_{ij}^2}^3} \times \left(1 - \frac{3\varepsilon^2(e^2 - s'^2)}{2\{(s-s')^2 + d_{ij}^2\}}\right) \right. \\ &+ \left(1 + \frac{d_{ij}^2}{\{(s-s')^2 + d_{ij}^2\}} \left[1 - \frac{3\varepsilon^2(e^2 - s'^2)}{2\{(s-s')^2 + d_{ij}^2\}}\right]\right) \\ &\left. \times \frac{\alpha_j^b(s')}{\sqrt{(s-s')^2 + d_{ij}^2}} \right\} \mathrm{d}s' \\ &+ \frac{\varepsilon^2}{2} \sum_{\substack{j=1 \\ j \neq i}}^{m} \int_{-e}^{e} \frac{(e^2 - s'^2)\alpha_j^b(s')}{\sqrt{(s-s')^2 + d_{ij}^2}^3}\, \mathrm{d}s' \qquad i = 1, \ldots, m \end{aligned} \tag{7}$$

where $L = \ell_n(2/\varepsilon)$.

Having obtained the intensities of the singularities, we now calculate the flowfield around the row. Most of the fluid moves around the edges of the finite row, but some penetrates between row members. The penetrating flow causes a shear force on the body in the direction of the flow and linearly proportional to the speed.

The force exerted on the ith rod is

$$D_i^j = 8\pi\mu \int_{-e}^{e} \alpha_i^j(s)\,\mathrm{d}s \tag{8}$$

where $j = n, s, b$ and $i = 1, \ldots, m$. The forces calculated are directly proportional to the leakiness (the ratio of the penetrating fluid mass flux and the undisturbed flux) of the row, which itself is proportional to the loss of force of the comb wing relative to the full wing of the same covered area.

The normal velocity at a point (x, y, z) of the ambient fluid, which is at distance $\mathbf{r} = (r_s, r_n, r_b)$ from point s on the axis of any rod, is

$$u(x,y,z) = \sum_{i=1}^{m} \int_{-e}^{e} \alpha_i^n(s)\left[\frac{1}{r} + \frac{2r_n^2 + \varepsilon^2(e^2 - s^2)}{2r^3} - \frac{3\varepsilon^2(e^2 - s^2)r_n^2}{2r^5}\right]\mathrm{d}s \tag{9}$$

The tangential and binormal velocity components can be calculated in likewise manner.

III. Results

The difference in the forces between a row of rods that move with uniform speed and one with velocities growing linearly with distance from the shoulder with average speed equal to the uniform speed is shown in Fig. 3. Here we used the data for the wing of our gliding UAV [10], that is, 1.5×10^{-3} m span and 2×10^{-3} m chord. The rods are of length 2×10^{-3} m (wing chord) and 5×10^{-6} m (maximal diameter). The interrod spacing d is 25×10^{-6} m.

The total force on the row is almost the same for the two cases, as the aerodynamic forces produced in creeping flow are linearly dependent on the velocity. However, the distribution of the forces within the row is completely different. In the symmetrical situation [3], the force is minimal at the central part of the uniformly moving row, as most of the flow is deflected around the row as a whole. Losses appear mainly near the ends of the row. For the present case, we obtain a monotonic, highly nonlinear distribution of forces. The slower rods are essentially carried along by the flow generated by the other rods. Thus, an opposite force is required to slow them down (Fig. 3).

In an optimally designed wing, we would like to use as few rods as possible (to reduce the total weight) per unit total force obtained on the wing. Thus, one should omit every rod that does not contribute, or contributes little, to the total force, like the rods close to the shoulder. Next, we compare wings of given span and fixed rod spacing, with a varying number of rods, obtained by having the rods placed at different distances from the shoulder.

The first case is of a wing with rods distributed evenly from the shoulder all the way to the wingtip, which has 60 evenly spaced rods. The first rod is taken to have an average nondimensional speed of 0.016 and the speed of consecutive rods is greater by the same increment, so that the tip velocity is unity and the average velocity is 0.5. The normal force distribution appears in Fig. 4, where the abscissa indicates the rod number, counting from the shoulder outwards toward the wingtip. The ordinate shows the force on the rod divided by the force on a single rod of equal dimensions moving at the same speed around the shoulder axis. Thus, the fact that the numbers are much smaller means that the relative speed each rod experiences is close to zero, that is, that of a continuous wing. The 15 rods closest to the shoulder actually move more slowly than the flow around them and, actually, as mentioned previously, reduce the total force produced during the downstroke.

This is compared in Fig. 4 to wings of equal span, comprising 50, 40, 30, 20, and even 10 rods, equally spaced but starting further away from the shoulder, so that the slowest rod is moving at a larger speed

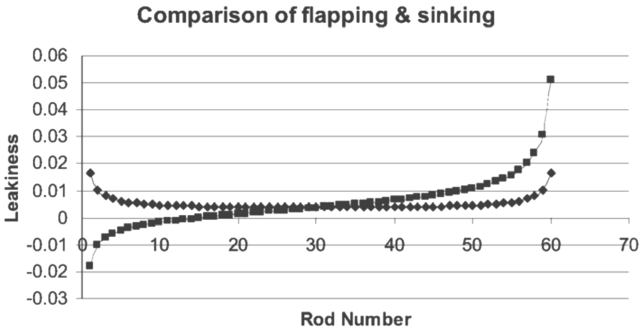

Fig. 3 Distribution of leakiness (losses relative to a full wing) as a function of spanwise position for a uniform velocity of 0.5 nondimensional units (diamonds), and for flapping, where the speed is in the range 0–1 (squares). The row has 60 rods, and rod no. 1 is closest to the shoulder.

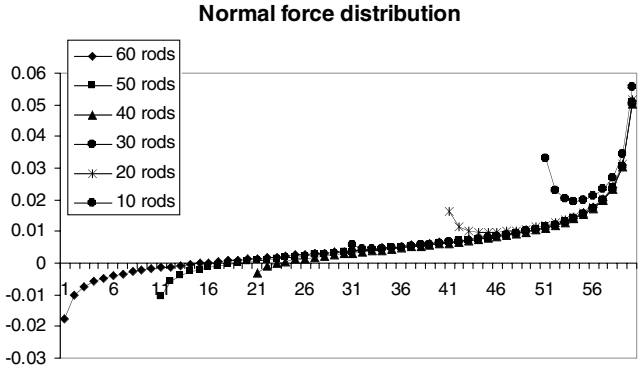

Fig. 4 Distribution of leakiness (losses relative to a full wing) as a function of spanwise position.

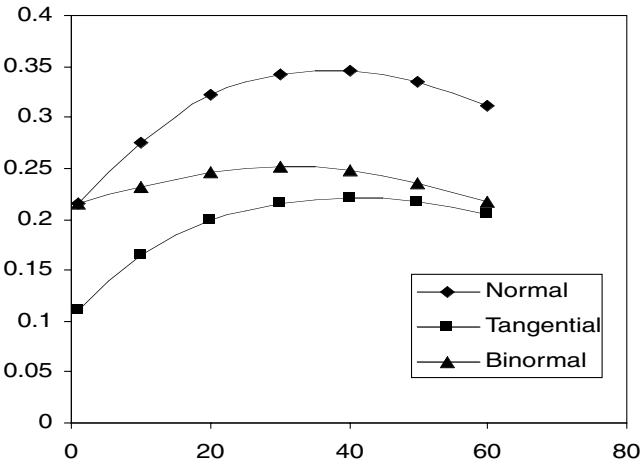

Fig. 5 Coefficients of hydrodynamic force in the three principal directions as a function of number of rods for the six wings described previously.

for arrays with less rods. The negative contribution of the slowest rods becomes less significant when the closest rod is farther away from the shoulder and vanishes altogether when the number of rods is 30 or less. Actually the "turning point" disappears for about 35 rods, but this is array dependent. Figure 4 also shows that the leakiness is identical for rods in the interior of the row, for all except the 10 rod wing. The latter does not have rods enough to constitute a "center."

The magnitude of the effect of eliminating the rods closest to the shoulder depends on the direction of motion but is qualitatively the same for all directions. Figure 5 shows the nondimensional values of the coefficients for the three major directions, normal, tangential and binormal, for the six configurations described above.

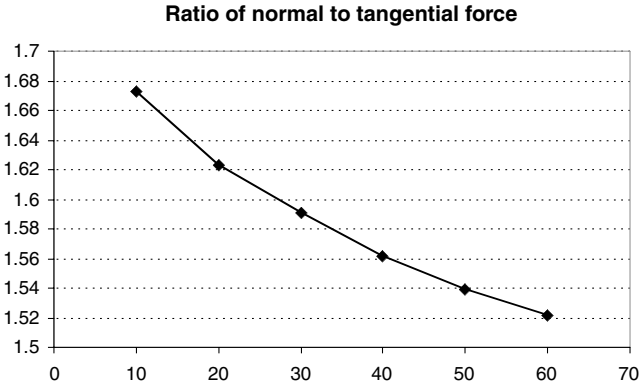

Fig. 6 Ratio of normal to tangential force produced by the wings described in previous figures.

The 30 rod wing has the best performance, that is, the best combination of forces in the normal direction and ratio (Fig. 6) of normal to tangential speed. For a single rod, extrapolation of the curves gives the classical result of the normal force being approximately twice the tangential force. Also, for a single rod, the force in the binormal direction is identical to the normal force for a rotationally symmetric body. For large numbers of rods, the binormal force tends to approach the tangential coefficient. This trend can be explained by the fact that for a row with large numbers of rods, flow in the binormal direction "sees" an almost continuous surface thus approaching the situation for tangential flow.

For flapping wings, the simplest model of the power stroke is motion of the rods along the normal direction while one of their ends is fixed ($u = 0$) with linearly increasing velocity. The simplest recovery stroke consists of feathered motion in the tangential direction. And so, for net flapping cycle downward force, the ratio between these two forces will determine the effectiveness. Figure 6 shows that about 60–65% of the downward force was lost on the recovery stroke.

More complex motions probably improve the ratio between the forces gained by the power stroke and lost by the recovery stroke.

IV. Conclusions

In a previous paper [3], we developed the method of calculating creeping flow around rows of slender ellipsoids by means of the distribution of singularities along the centerlines of these bodies. The present paper applies this to flapping wings. Our results indicate that the part of the span closest to the shoulder is ineffective and can even hinder the movement. This prediction is supported by the fact that insect wings (see Fig. 1) do not have bristles close to the shoulder, and the nearest bristles are of smaller size. Naveh et al. [10] constructed a nano-UAV with bristled wings, saving much weight. Our results indicate that such a wing acts almost as a full wing. Thus, the reduction of weight is a pure gain in effectiveness.

Extensions of the present work, such as nonlinear variation of speed in the spanwise direction and flexibility of the wing, can better simulate motion of a bristled comb wing [2,11] and are relatively simple to accomplish. For example, spanwise flexibility is modeled by having the rods positioned along a curved surface instead of being in a plane. Angles of attack (AOA) and sideslip are treated by breaking up the velocity into two (AOA) or three (sideslip) components to obtain the singularity distribution. Dealing with several dozen bodies simultaneously, and considering the fact that we cannot use symmetrical distributions of intensities as in the uniform velocity case, we had to reduce the number of numerical net points to enable a solution. However, we validated (by comparing solutions obtained for several numerical grids) that our solution converges even for sparse grids, for example, 50 points are sufficient to accurately describe a slender body of ratio > 100. In general, there was no other way to be sure that the errors involved with our computations are reasonably low but to check the deviation of the velocity induced by our computed solution with the dictated no-slip velocity. The degree of inaccuracy was shown to be less than 3% for the various cases solved. For the aforementioned example, we found that the highest relative errors of the velocity are obtained at the tips of the ellipsoids at the shoulder end of the row ($<2.5\%$ for both normal and binormal directions). The forces are small anyway in that region. The errors quickly decrease to 0.5% (and even less) towards the "faster half" of the body and towards the center of the wing.

Unfortunately, there is almost no data available concerning the exact structure and motion of wings of the miniature insects that have comb wings. Once such data is available, it might be beneficial to formulate a model for more complicated or nonuniform situations within the row, for example, velocity that changes in a nonlinear fashion along the axis or row, or other shapes of slender bodies. Thus, flapping wing, highly efficient and extremely light nano-UAVs based on comb wings will be possible.

Acknowledgments

This study was partly funded by the Deborah Fund at Technion. We thank Shlomit Gali for her support.

References

[1] Zussman, E., Yarin, A. L., and Weihs, D., "A Micro-Aerodynamic Decelerator Based on Permeable Surfaces of Nanofiber Mats," *Experiments in Fluids*, Vol. 33, No. 2, 2002, pp. 315–320. doi:10.1007/s0034800204356

[2] Sunada, S., Takashima, H., Hattori, T., Yasuda, K., and Kawachi, K., "Fluid-Dynamic Characteristics of a Bristled Wing," *Journal of Experimental Biology*, Vol. 205, No. 17, Sept. 2002, pp. 2737–2744.

[3] Barta, E., and Weihs, D., "Creeping Flow Around a Finite Row of Slender Bodies in Close Proximity," *Journal of Fluid Mechanics*, Vol. 551, March 2006, pp. 1–17. doi:10.1017/S0022112005008268

[4] Tamada, K., and Fujikawa, H., *Quarterly Journal of Mechanics and Applied Mathematics*, Vol. 10, No. 3, 1957, pp. 425–431. doi:10.1093/qjmam/10.4.425

[5] Cheer, A. Y. L., and Koehl, M. A. R., "Paddles and Rakes: Fluid Flow Through Bristled Appendages of Small Organisms," *Journal of Theoretical Biology*, Vol. 129, No. 1, 1987, pp. 17–39. doi:10.1016/S0022-5193(87)80201-1

[6] Ayaz, F., and Pedley, T. J., "Flow Through and Particle Interception by an Infinite Array of Closely-Spaced Circular Cylinders," *European Journal of Mechanics, B/Fluids*, Vol. 18, No. 2, 1999, pp. 173–196. doi:10.1016/S0997-7546(99)80021-1

[7] Ellington, C. P., "The Novel Aerodynamics of Insect Flight: Applications to Micro-Air Vehicles," *Journal of Experimental Biology*, Vol. 202, No. 23, Dec. 1999, pp. 3439–3448.

[8] Happel, J., and Brenner, H., *Low Reynolds Number Hydrodynamics*, Noordhoff International, Leyden, The Netherlands, 1973, p. 225.

[9] Barta, E., and Liron, N., "Slender Body Interactions for Low Reynolds Numbers, Pt. 2: Body-Body Interactions," *SIAM Journal on Applied Mathematics*, Vol. 48, No. 6, Dec. 1988, pp. 1262–1280. doi:10.1137/0148077

[10] Naveh, R., Yechieli, R., Sachyani, M., and Weihs, D., "MEMS Based Structure For Miniature Aerial System," ISRAMEMS Paper 5-2003, 2003.

[11] Kuethe, A. M, "On the Mechanics of Flight Insects," *Swimming & Flying in Nature*, edited by T. Y. Wu, C. J. Brokaw, and C. Brennen, Vol. 2, Plenum, New York, 1975, pp. 803–813.

A. Plotkin
Associate Editor